Available online at www.sciencedirect.com
ScienceDirect
Journal of Sound and Vibration 321 (2009) 1109–1128
JOURNAL OF SOUND AND VIBRATION
www.elsevier.com/locate/jsvi

Time–frequency features of two types of coupled rub-impact faults in rotor systems

Hui Ma[a,*], Tao Yu[b,c], Qingkai Han[a], Yimin Zhang[a], Bangchun Wen[a], Chen Xuelian[d]

[a]School of Mechanical and Automation, Northeastern University, Shenyang, Liaoning 110004, PR China
[b]Center for Noise and Vibration Control (NOVIC), Department of Mechanical Engineering, KAIST, Science Town, Daejeon 305-701, Republic of Korea
[c]School of Electromechanical Automobile Engineering, Yantai University, Yantai, Shandong 264005, PR China
[d]Shen Yang Institute of Automation, Chinese Academy of Sciences, Shenyang, Liaoning 110016, PR China

Received 18 November 2006; received in revised form 25 July 2008; accepted 30 September 2008
Handling Editor: J. Lam
Available online 28 November 2008

Abstract

Two types of rub-impact faults in rotor systems are studied in this paper. First is crack coupled with rub-impact, and second is oil-film instability coupled with bearing rub-impact. By combining spectrum cascade, reassigned wavelet scalogram, rotor trajectory, and frequency spectrum, some novel fault features have been discovered from the vibration signals measured in both the speeding up and slowing down process. The results show that for crack coupled with rub-impact fault, the system motion is from period-three motion, to period-two motion, then to period-four motion in the slight rub-impact stage. However, in the stage of the serious rub-impact, chaotic motion occurs. For oil-film instability coupled with rub-impact fault, rotational frequency, oil-film instability frequency, and the combined frequencies of them can be observed when slight bearing rub-impact occurs. When bearing rub-impact is increasingly serious, the increase of low frequency amplitude can be viewed as the most distinguishable characteristic.

1. Introduction

Rotor-to-stator rub-impact is a type of serious fault occurring often in rotating machinery. So far, rub-impact fault alone has been studied extensively, using various research methods. Muszynska [1] discussed chaotic responses of unbalanced rotor-bearing-stator systems with rubbing. The results showed that at low rotational speeds, the rotor's response exhibits $1X$ vibration as the lowest frequency component. At a speed roughly equal to twice the rotor's first lateral natural frequency, a $1X/2$ sub-synchronous vibration component appears, and continues until the rotational speed reaches 3 times the rotor's first natural frequency. Then, the $1X/2$ is replaced by $1X/3$ vibration as the lowest frequency component. Muszynska also pointed out that there

*Corresponding author. Tel.: +86 24 83671429; fax: +86 24 83679731.
E-mail address: mahui_2007@163.com (H. Ma).

0022-460X/$ - see front matter © 2008 Elsevier Ltd. All rights reserved.
doi:10.1016/j.jsv.2008.09.054

is evidence of rotor chaotic responses at some speeds. Zhang [2] presented a rub-impact micro-rotor model with scaling nonlinear rub-impact force and the nonlinear dynamic characteristics of micro-electro-mechanical systems (MEMS) were investigated when the rotational speed, imbalance, damping coefficient, scale length, and fractal dimension are regarded as the control parameters. Piccoli and Weber [3] conducted an experiment to observe chaotic motion in a rubbing rotor system. The work concluded that the possibility of chaotic motion is well determined with the observation of Poincare diagrams and computation of Lyapunov exponents. Chu and Lu [4] studied the nonlinear vibration of a rub-impact rotor system and observed a variety of periodic and chaotic vibrations. The experiments showed that the system motion generally contains multiple harmonic components, such as $2X$, $3X$, and $\frac{1}{2}$-based fractional harmonic components, such as $1X/2$ and $3X/2$. Under some special conditions, the $\frac{1}{3}$-based fractional harmonic components can also be observed. Dai et al. [5] designed an experiment involving rotor-stop rubbing, and analyzed its vibration responses. The experiment showed that when the amplitude of the excitation force exceeds a certain value, full rubbing occurs with serious continuous friction. During the full rubbing, the rotor orbit moves counter-clockwise and the whip amplitude abruptly exceeds the rotor-stop gap.

Under many circumstances, the rub-impact is usually a secondary phenomenon resulting from excessive vibration caused by other faults in the practical rotor systems, such as rotor crack, oil-film instability, and pedestal looseness. Though research on coupled rub-impact faults is very important, not enough research has been done in this area. Bachschmid et al. [6] presented a model-based identification method for multiple faults. Some numerical simulations were reported for two simultaneous faults and experimental results obtained on a test rig were used to validate the identification procedure. The experimental results prove that the method is effective in identifying both the faults in position, module, and phase. Luo et al. [7] set up a dynamic model for a rotor-bearing system with crack coupled with rub-impact fault. The results showed that there are peculiar dynamic characteristics of the rotor-bearing system with crack coupled with rub-impact fault that differ from that with only one kind of fault. Wen and his team [8] studied the dynamic characteristics of a rotor-bearing system with crack coupled with rub-impact fault, by taking the effects of imbalance, crack angle, and rotor-to-stator clearance into consideration. Wan [9] investigated the vibration of a cracked rotor sliding bearing system with rotor-stator rubbing, by using the harmonic wavelet transform (HWT) method. Wu and Meng [10] extracted the features of some typical compound rub malfunctions, by using full-spectrum cascade analysis and SVM. The results showed that when the rotor does not touch the stator, there is a free vibration with decaying damp aroused by the rub; the inherent frequency of the rotor system would emerge in the frequency spectrum plot. If the rub range is small, the amplitude of $1X$ is stable and the harmonics spectrum is less. If the rub is heavy, the amplitude of $1X$ decreases, more harmonic components will be produced, and the frequency spectrum energy scatters further.

Research proved that vibration signals are non-stationary and time-varying due to the change of rotational speed and the nonlinear vibration characteristics of a rotor system with faults in both the speeding up and slowing down process. To process this kind of signal, time–frequency analysis, such as wavelet transform (WT), is adopted widely. Peng [11] presented a comparison of the performances of the different time–frequency methods and pointed out the advantages of the wavelet analysis in analyzing non-stationary signals. Auger and Flandrin [12,13] improved the readability of time–frequency and time-scale representation by introducing the reassigned method. Improved scalogram has the property of concentrating the detected signals in their respective frequencies and time locations. So the reassigned method can reduce cross-terms and improve time–frequency resolution. Han [14] performed an experiment to investigate the instable vibration behaviors of oil-film whirl on a rotor test rig. The rotor shaft vibrations in steady and run up–down processes are measured and analyzed by using the WT technique and a wavelet-fractal method. Adewusi and Al-bedoor [15] used the wavelet analysis method to extract the fault features of an overhang rotor with a propagating transverse crack. The results revealed that the fault features could be well extracted under the condition of start-up and steady-state vibration by the wavelet analysis. Darpe [16] presented a novel way to detect fatigue transverse cracks in rotating shafts. He used WTs to reveal the transient features of the resonant bending vibrations, which were set up for a short duration of time upon transient torsional excitation. Yang et al. [17] presented the results of detecting, identifying, and characterizing the dynamical states of a cracked rotor-bearing system by using the discrete WT and the concept of energy variation. A wavelet-based algorithm was developed successfully to characterize periodic, period-doubling, fractal-like, and chaotic motions as the result

of the inherent nonlinearity (nonlinear stiffness) associated with crack openings and closings during vibration. Tse et al. [18] diagnosed the bearing fault by using the wavelet analysis and envelope detecting method. The results showed that if high energy impacts are observed in the high frequency range in the time–frequency distribution diagram, then the faults can be identified in the bearing. Additional evidence to prove the existence of faults in a rotor system can be obtained by inspecting whether a substantial increase of vibration energy is found in the low frequency range of the time–frequency distribution diagram. By inspecting the time interval of the impacts in the high frequency bearing excitation range, the cause of a fault can be identified. By using scalograms, Peng et al. [19,20] analyzed three kinds of typical faults: rub-impact, oil whirl, and coupling misalignment, all of which often occur in rotating machines. Further research on rubbing-caused impacts is carried out using the reassigned scalogram. The results indicated that the method of reassigned scalogram is much effective in identifying rubbing-caused impacts in both of the time and frequency domains.

The fault features of coupled rub-impacts are complicated due to the interaction of coupling factors. Most of the previous research was focused on numerical simulations, and the corresponding experimental verification was insufficient. In our research, the experiments on crack or oil-film instability coupled with rub-impact have been carried out on a rotor test rig. The rough time–frequency features can be observed by using spectrum cascade and the detailed time–frequency features were obtained by using the reassigned wavelet scalogram, rotor trajectory, and frequency spectrum. The results presented some particular fault features that can be viewed as proof of the occurrence of the corresponding fault in the rotor system.

In our study, the combination of spectrum cascade, reassigned wavelet scalogram, rotor trajectory, and frequency spectrum has been used to analyze the two types of coupled rub-impact faults. Some novel and interesting phenomena have been observed. What should be pointed out is that the study shown in this paper is mainly focused on the coupled rub-impact faults but not on the advantages of the reassigned scalogram or other time–frequency methods. The advantages of the combined use of several time–frequency methods in this investigation show us it is impossible to reveal the coupled rub-impact faults with only one single time–frequency method. The results may give references to the studies of other coupled faults in rotor systems.

The principle of the reassigned wavelet scalogram is briefly discussed in Section 2. Section 3 introduces the setup of the rotor system, rub-impact device and crack shaft machining, and experimental parameters' description. In Section 4, rough time–frequency features of crack, rub-impact, and coupling fault of both are analyzed in Section 4.1; fault features of the rub-impact alone and the crack coupled with rub-impact are analyzed in Sections 4.2 and 4.3, respectively; the fault feature comparison of single and coupled rub-impact is described in Section 4.4. In Section 5, the fault features of the oil-film instability coupled with rub-impact are analyzed. The conclusions of this paper are given in Section 6.

2. The reassigned wavelet scalogram

Assume $x(\tau)$ to be a finite-energy function, that is, $x(\tau) \in L^2(R)$. If Fourier transform $\hat{h}(f)$ meets the admissibility condition: $C_h = \int_{-\infty}^{+\infty} |\hat{h}(f)|^2/|f|\,\mathrm{d}f < \infty$, $h(\tau)$ is called mother wavelet. The family of wavelet $h_{t,a}(\tau)$ consists of a series of son wavelets, which are generated by dilation and translation from the mother wavelet $h(\tau)$, as shown in the following: $h_{t,a}(\tau) = (1/\sqrt{a})h(\tau - t/a)$. For any function $x(\tau) \in L^2(R)$, the WT is defined as

$$CWT_x(t,a;h) = \int_{-\infty}^{+\infty} x(\tau) h^*_{t,a}(\tau)\,\mathrm{d}\tau, \tag{1}$$

where t is the time parameter, a is the scale parameter, $h^*_{t,a}(\tau)$ is the conjugate function of $h_{t,a}(\tau)$, and $1/\sqrt{a}$ is used to ensure conservation of energy.

For all $h(\tau), x(\tau) \in L^2(R)$, the continuous inverse WT $x(\tau)$ is defined as

$$x(\tau) = \frac{1}{C_h} \int_{-\infty}^{\infty} \int_{-\infty}^{\infty} a^{-2} CWT_x(t,a;h) h_{t,a}(\tau)\,\mathrm{d}t\,\mathrm{d}a. \tag{2}$$

Eq. (2) shows clearly that the wavelet transformation does not lose any information, and the energy is conservative for the transformation. So the following equation is tenable:

$$\int_{-\infty}^{\infty} |x(\tau)|^2 \, \mathrm{d}\tau = \frac{1}{C_h} \int_{-\infty}^{\infty} a^{-2} \, \mathrm{d}a \int_{-\infty}^{\infty} |CWT_x(t,a;h)|^2 \, \mathrm{d}t. \tag{3}$$

$SCAL_x(t,a;h) = |CWT_x(t,a;h)|^2$ is defined as the wavelet scalogram. For the limitation of Heisenberg–Garbor inequality, time and frequency resolutions of the scalogram cannot be obtained at the same window defined in the time–frequency plane.

To overcome the defects of conventional wavelet scalogram, Auger and Flandrin [12,13] developed the reassigned wavelet scalogram, which has better time and frequency concentration and less interference, compared with the conventional wavelet transformation. The reassigned method can shift the components from the geometrical center of the window of the timescale analysis to the gravity center of their complex energy density distribution. Since the energy density contained in the components of the reassigned scalogram has little deviation from that in the original signals and thus suffers less interference, even components containing low energy can be identified in the reassigned scalogram, as depicted in Fig. 1, where the ellipse is a resolution window of wavelet whose geometrical center is (t,f). According to the definition of the wavelet scalogram, $|CWT_x(t,a;h)|^2$ represents the average energy of the resolution window, but actually, there is no energy at the geometrical center of the resolution window. Obviously, this averaging will lead to poor concentration, hence, to interference terms. One way to avoid this is to change the contribution point of this average and reassign it to the center $(\hat{t},\hat{f})$ of the gravity of these energy distributions. The detailed information about reassigned wavelet scalogram and its algorithm can be found in Refs. [12,13].

3. Experimental setup

3.1. Experiment arrangement of the rotor system

The rotor test rig, as shown in Fig. 2, is composed of a motor, a flexible coupling, a sliding bearing/a graphite bearing, a shaft, and a disc. The diameter and width of the disc are 80 and 20 mm, respectively. The shaft was changed in different experiments. The diameter and length of the shaft are 10 and 400 mm in the crack coupled with rub-impact experiment. In the experiment of the oil-film instability coupled with rub-impact, we used a stepped shaft with a total length of 300 mm, whose diameter varies from 25 to 10 mm in the axial location of 30 mm from the left end in Fig. 2. The diameter of the sliding bearing is 25.18 mm and its width is 8 mm. Number 30 lubrication oil was adopted. The motor and the rotor system were connected by a

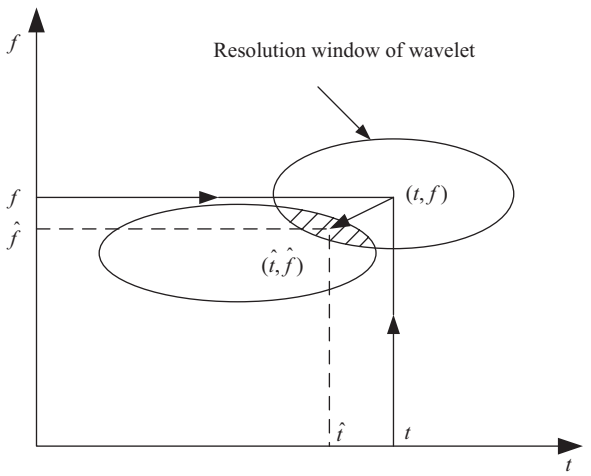

Fig. 1. Energy distribution of an illustrated signal.

flexible coupling to reduce the effect of the motor on the rotor system. Two eddy current proximity probes were mounted to measure the vibration displacements of the shaft in horizontal direction x and vertical direction y, as shown in Fig. 2. The sampling frequency was 2000 Hz.

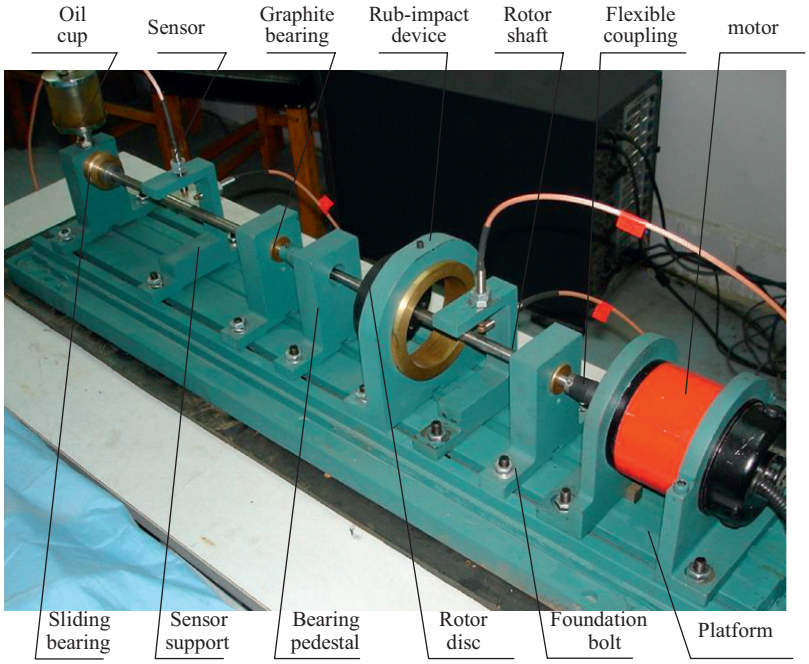

Fig. 2. Rotor test rig.

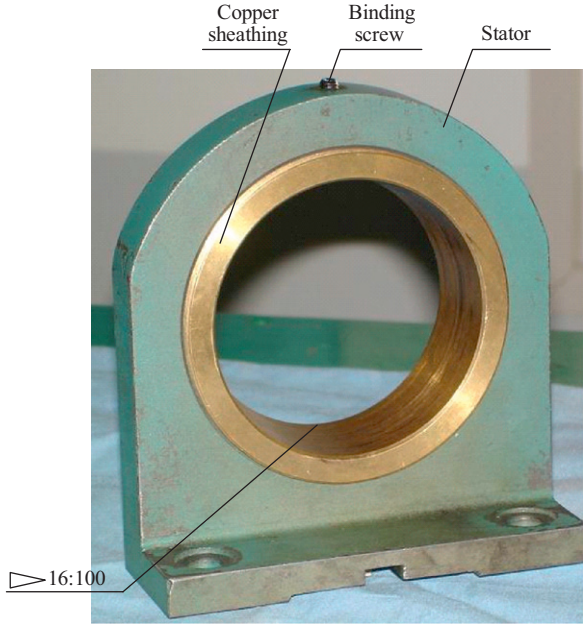

Fig. 3. Rub-impact device.

3.2. Rub-impact device and cracked shaft machining

In order to well simulate rub-impact fault that often occurs in practical rotor systems, a special rub-impact device was designed, as shown in Fig. 3. The stator is made of a steel plate of 5 mm thickness, with a central hole whose inner diameter is slightly larger than that of the disc. A cone-shaped copper sheathing with a taper of 16:100 is embedded in its central hole as rub-impact surface. The stator can be moved along the centerline of the shaft from left to right, so the rotor-to-stator clearance can be adjusted from 0 to 2 mm. The device can well simulate the real rub-impact process because of convenient clearance adjustment. As to the cracked shaft, a transverse crack with moderate depth was introduced on the shaft.

3.3. Experimental parameter description of the two types of coupled rub-impact faults

For the experiment of the crack coupled with rub-impact, called the first experiment here, the following sub-experiments were performed: experiment with only rotor crack, experiment with only rotor-to-stator rub-impact, and experiment with crack coupled rub-impact. A graphite bearing was adopted in the first experiment. The sketch of the rotor system is shown in Fig. 4. The main parameters of the system were as follows: disc mass $m = 0.736$ kg, bearing span $l = 360$ mm, eccentric mass $m_1 = 0.82$ g, eccentricity $e = 34.35$ mm. The first critical speed was about 3100 rev/min. For fault feature comparison of crack, rub-impact, and their coupling, crack fault was simulated by removing the rub-impact device and rub-impact fault was simulated by changing the normal shaft.

The second experiment was carried out to simulate the oil-film instability coupled with bearing rub-impact fault. For this purpose, the right bearing was replaced by a sliding bearing. The sketch of the rotor system with oil-film instability coupled with bearing rub-impact fault is shown in Fig. 5. The main parameters of the system were as follows: disc mass $m = 0.736$ kg, bearing span $l = 280$ mm, eccentric mass $m_1 = 0.48$ g, eccentricity $e = 34.35$ mm. The first critical speed was about 4800 rev/min.

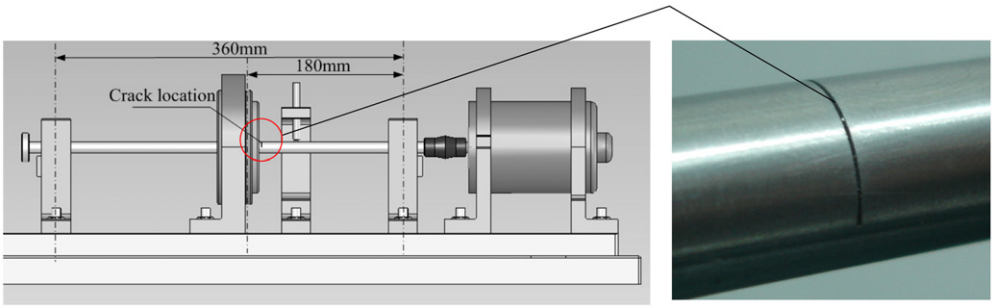

Fig. 4. The rotor system with crack coupled with rub-impact faults.

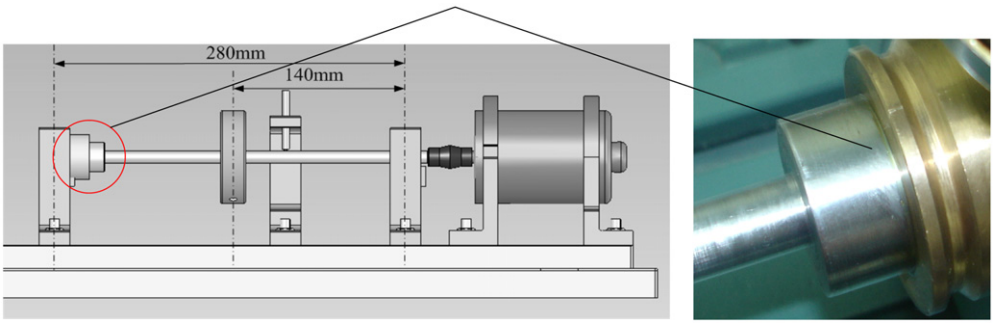

Fig. 5. The rotor system with oil-film instability coupled with bearing rub-impact faults.

4. Time–frequency features of crack coupled with rub-impact faults

By combining spectrum cascade, reassigned wavelet scalogram, rotor trajectory, and frequency spectrum, the fault features of the crack coupled with rub-impact have been obtained from the vibration signals measured in both the speeding up and slowing down process.

4.1. Rough time–frequency features of crack, rub-impact and coupling of both

Figs. 6(a)–(c) show the spectrum cascades of the rotor system with crack, rub-impact and coupled fault of both in both the speeding up and slowing down process. The regular rotational frequency $1X$ and second harmonic component $2X$ can be observed in Fig. 6(a), which is in agreement with results in Refs. [21–23]. Besides $1X$, the higher frequency components near the critical speed can be observed in Fig. 6(b). Fig. 6(c) shows that $2X$ is more obvious and the frequency components near the critical speed are more complicated than those in Fig. 6(b). For crack fault, the time–frequency features can be observed by using spectrum cascade, but fault features of single rub-impact and crack coupled with rub-impact are more complicated and cannot be clearly observed by using the spectrum cascades alone. So in order to better observe fault features,

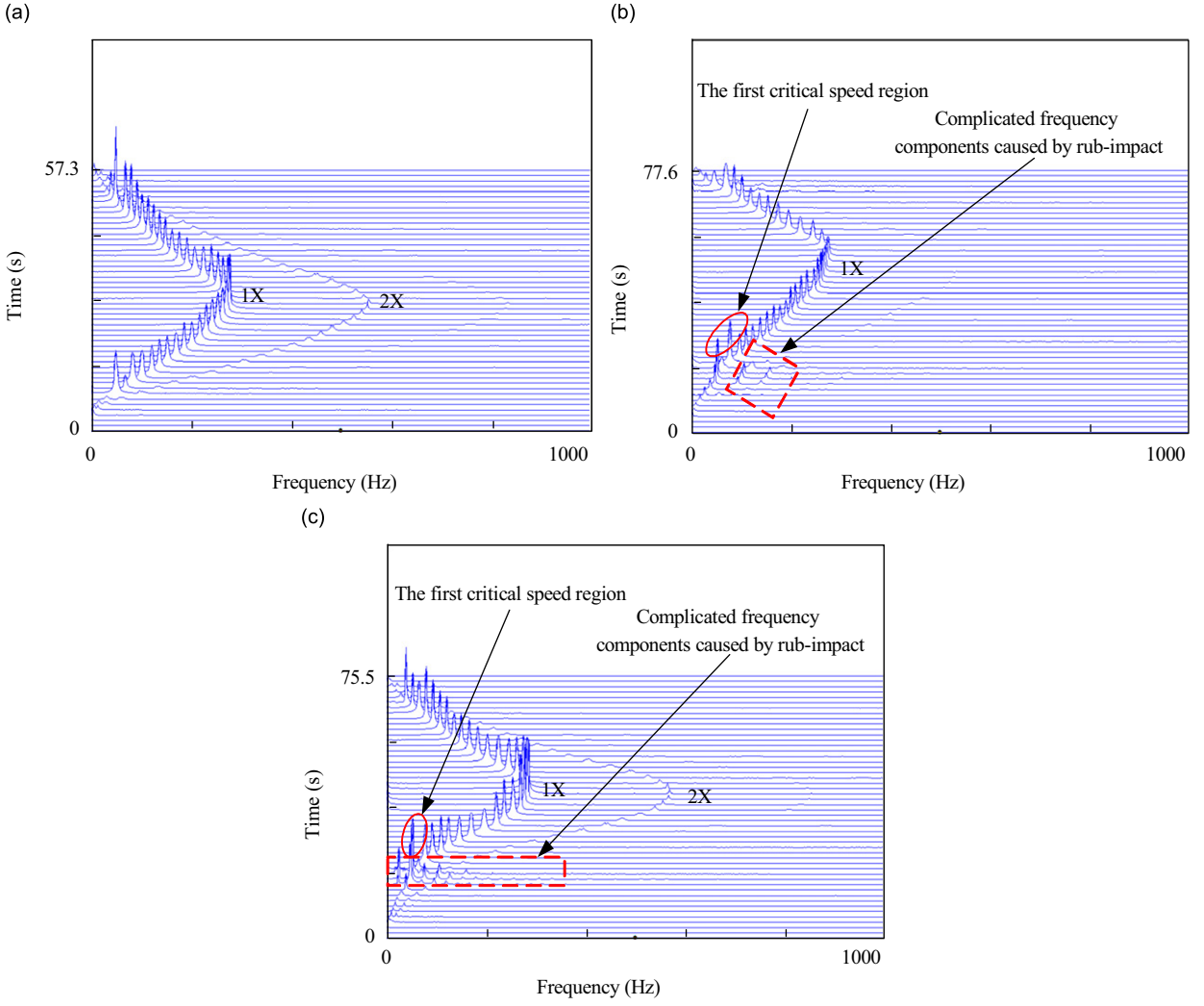

Fig. 6. Spectrum cascades of crack, rub-impact and coupling faults of both in both the speeding up and slowing down process: (a) crack fault, (b) rub-impact fault, and (c) crack coupled with rub-impact.

Table 1
Figure description of the rub-impact fault.

Analysis method	Figures order number	Time range (s)	Rotational speed range (rev/min)
Spectrum cascade	Fig. 6(b)	0–77.6	0–16500
	Fig. 9	14.5–18.5	2855–3398
Reassigned wavelet scalogram	Fig. 7(a)	10.5–11.5	1436–1846
	Fig. 7(b)	11.5–12.5	1846–2227
	Fig. 7(c)	14.5–15.5	2855–2988
	Fig. 7(d)	17.5–18.5	3164–3398
	Fig. 7(e)	18.5–19.5	3398–4102
Rotor trajectory	Fig. 8(a)	10.5–11.5	1436–1846
	Fig. 8(b)	11.5–12.5	1846–2227
	Fig. 8(c)	17.5–18.5	3164–3398
	Fig. 8(d)	19.5–20.5	4102–4629

the reassigned wavelet scalogram has been adopted to analyze the single rub-impact and coupled rub-impact vibration signals near the critical speed.

4.2. Detailed time–frequency features of single rub-impact fault

An experimental description of all figures about the rub-impact fault is shown in Table 1.

The complete process of the single rub-impact fault from occurring to aggravating can be observed in Fig. 7(a). At the beginning stage, only the $1X$ and $2X$ harmonic frequencies can be observed when there is no rub-impact. When the rotational speed reaches about 1535 rev/min (10.74 s), the continuous $3X$, $4X$ harmonic frequency bands and intermittent low energy impacts $5X$ can also be observed. The reason why the high frequency components and impacts occur is that the sudden appearance of the rotor-to-stator contact will cause a rapid change in the system momentum and will therefore lead to an impact on the system by introducing a broadband excitation. The truncation of the waveform becomes more serious, which also suggests the rub-impact worsening with the increase of rotational speed. In the period of the rotational speed from 1846 to 2227 rev/min, the vibration response of the system is shown in Fig. 7(b). Meanwhile, the $5X$ harmonic frequency is replaced by $6X$, which also suggests the impact caused by the rub-impact worsened continuously.

When the rotational speed is approaching the first critical speed, the rub-impact fault is more and more severe due to the appearance of the resonance, as shown in Fig. 7(c). At this time, the regular impacts disappear but the irregular spots appear from 14.5 to 15.1 s. The irregular spots are introduced by the colored noise caused by the rub-impact. Some low frequency components without a common divisor, which are called irreducible frequency components (IFC) in this paper, can be observed after 15.1 s. In other words, the system is in the state of quasi-periodic motion. When the rotational speed passes the critical speed, as shown in Fig. 7(d), the vibration displacement increases and the low harmonic frequency components are more complicated compared to those in Fig. 7(c). All of these features prove that the rub-impact fault becomes severe. The rotational speed at which the most serious rub-impact fault occurs is greater than the original critical speed because the critical speed increases during the contact period of the rotor and stator. Fig. 7(e) shows the process when the rub-impact gradually disappears. There are only the regular $1X$ and $2X$ harmonic frequencies when no rub-impact occurs. Fig. 8 shows the rotor trajectories in four different rotational speed ranges and the detailed parameter description is tabulated in Table 1. The rotor trajectory moves forward counter-clockwise, and the points 1 and 2 of trajectory move inwards and outwards, respectively, as shown in Fig. 8(a). The inner concave phenomenon shows the impact occurring. When the rub-impact worsens, the inner concave phenomenon is more and more obvious, as shown in Fig. 8(b), which also shows the violent

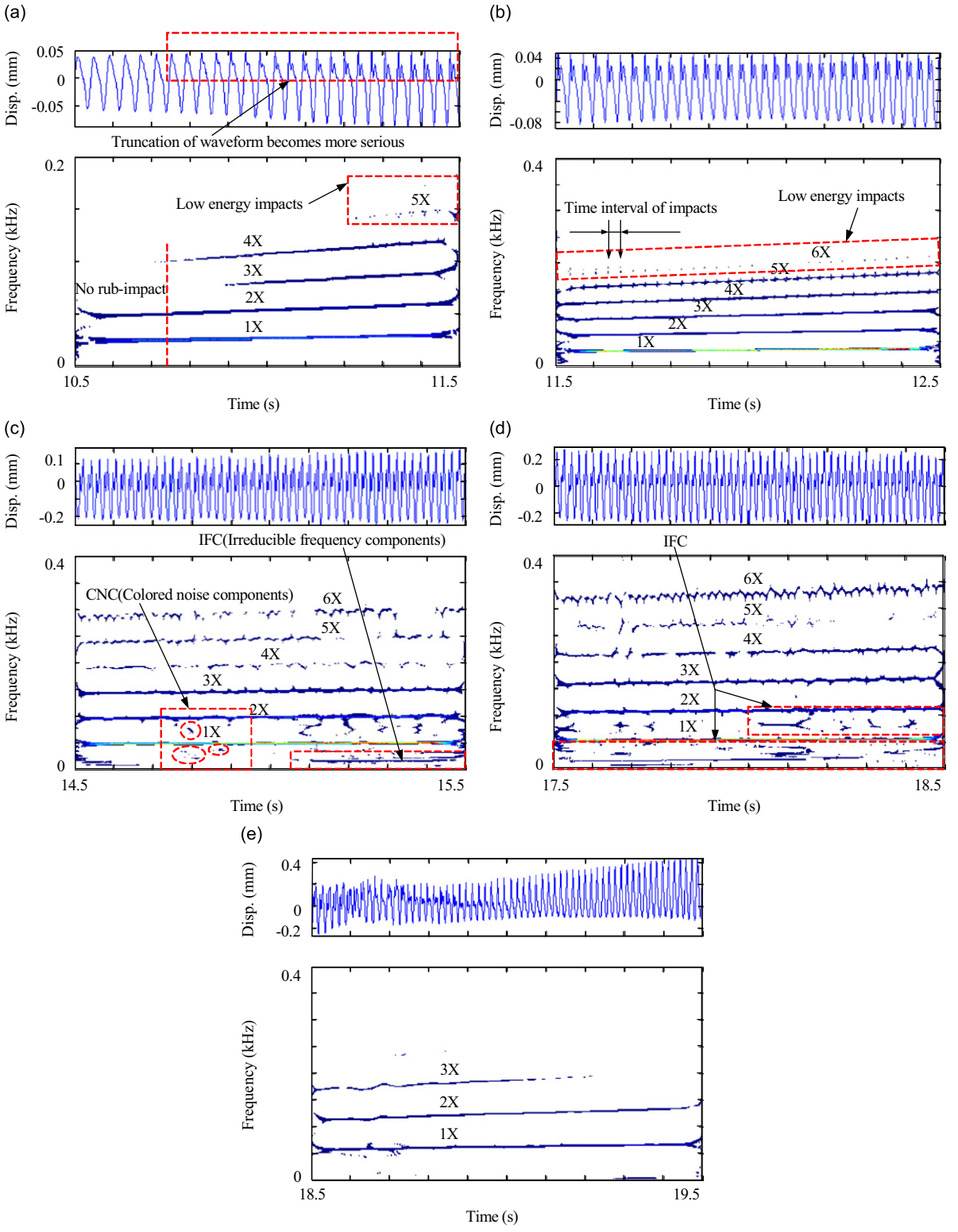

Fig. 7. Reassigned wavelet scalograms of rub-impact in different rotational speed ranges.

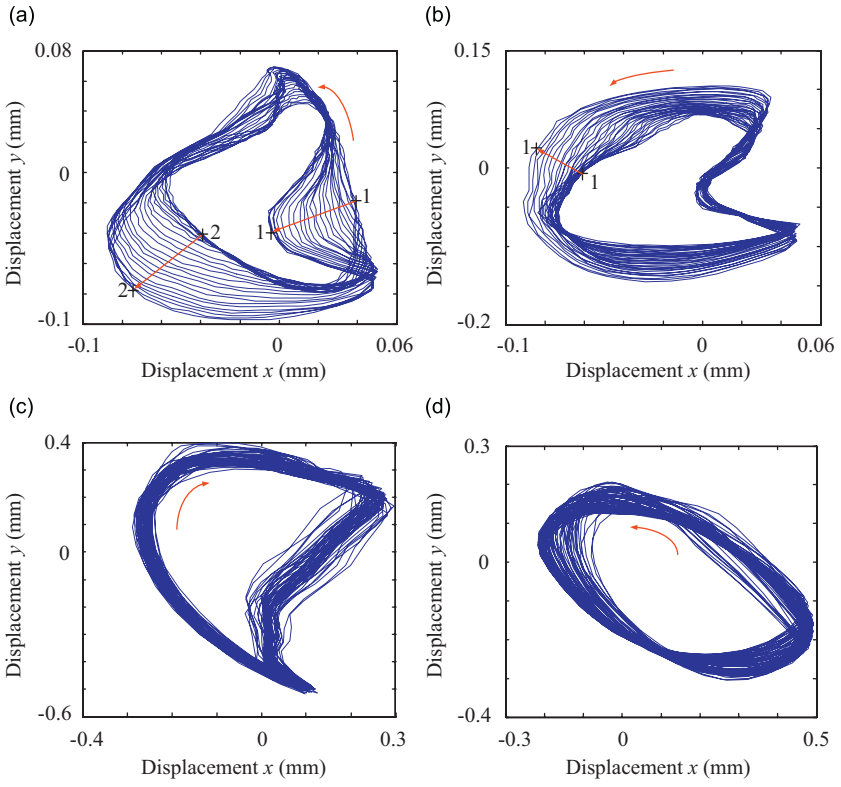

Fig. 8. Rotor trajectories with rubbing fault in four different rotational speed ranges.

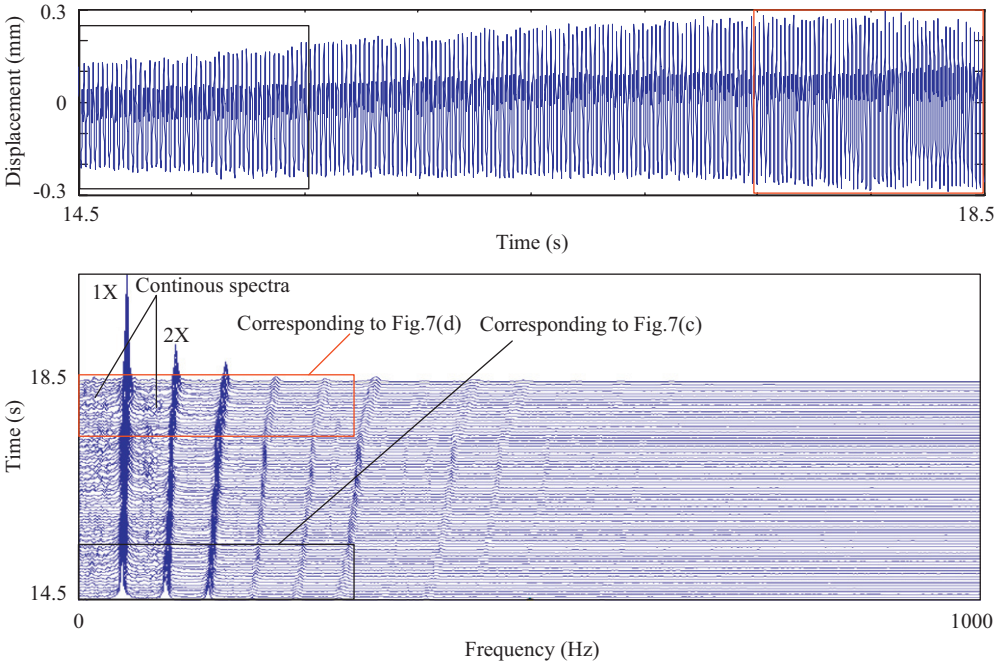

Fig. 9. Time-domain waveform and spectrum cascade in 14.5–18.5 s.

rebound of the impact. When the rub-impact becomes serious, the inner concave area increases and backward-precession occurs, as shown in Fig. 8(c). The rotor trajectory breaking away from the rub-impact is changed to ellipse and the motion direction is forward, as shown in Fig. 8(d).

Fig. 9 shows the time-domain waveform and spectrum cascade from 14.5 to 18.5 s. The displacement gradually increases, as shown in the time-domain waveform. The frequency features corresponding to Figs. 7(c) and (d) can also be observed in the spectrum cascade. By comparing these features, the result can be observed that the frequency composition of both is similar, but continuous spectrum amplitude, rotational frequency, and high frequency vibration amplitudes of the latter are greater than those of the former, which also shows that the rub-impact extent of the latter is more serious than that of the former.

4.3. Detailed time–frequency features of crack coupled with rub-impact fault

A description of the experiment involving crack coupled with rub-impact fault is tabulated in Table 2. Fig. 10(a) shows the process from single crack fault to crack coupled with rub-impact fault. There is only crack fault and the corresponding frequency component is $1X$ and $2X$ in 14.25–14.6 s. Slight rub-impact occurs near 14.6 s and the system motion is period-three (P3) motion. Meanwhile, $\frac{1}{3}$-based fractional harmonic components such as $1X/3$ and $2X/3$ can be observed, which shows that high energy impacts appear in high frequency domain. With the increase of rotational speed, the motion changes from period-three (P3) to period-two (P2) near 15 s. During period-two motion, the frequency spectrum is composed of $\frac{1}{2}$-based fractional harmonic components and impacts with higher frequency components occur, which can also be observed in Fig. 10(b). These higher frequency components occurring at 16.3 and 16.62 s, respectively, show that the impacts worsen when the rotational speed slowly increases, as shown in Fig. 10(c), which is consistent with the findings of the previous study sponsored by Peng [20]. By measuring the time interval of two adjacent impacts, the rub-impact period can be determined approximately. The rub-impact period is 38.4 ms and rotating period is about 19.2 ms, so the rub-impact occurs one time every two rotating periods, as shown in Fig. 10(d). When system motion changes from period-two (P2) to period-four (P4) and the irregular high frequency impacts occur, rub-impact becomes serious. After a short time of period-four (P4) motion, the system goes into a chaotic motion stage accompanied by very serious rub-impact, as shown in Fig. 10(e). With the increase of rotational speed, the system motion returns to period-one (P1) after coming through transitory chaotic motion, as shown in Fig. 10(f).

Table 2
Figure description of crack coupled with rub-impact.

Analysis method	Figures order number	Time range (s)	Rotational speed range (rev/min)
Spectrum cascade	Fig. 6(c)	0–75.5	0–17100
Reassigned wavelet scalogram	Fig. 10(a)	14.25–15.25	2490–2844
	Fig. 10(b)	15–16	2754–2988
	Fig. 10(c)	16–17	2988–3106
	Fig. 10(d)	17–18	3106–3164
	Fig. 10(e)	18–19	3164–3223
	Fig. 10(f)	19–20	3223–3985
Rotor trajectory	Fig. 11(a)	14–15	2402–2754
	Fig. 11(b)	16–17	2754–2988
	Fig. 11(c)	18–19	3164–3223
	Fig. 11(d)	19–20	3223–3985
Amplitude spectrum	Fig. 12(a)	17–18	3106–3164
	Fig. 12(b)	18–19	3164–3223

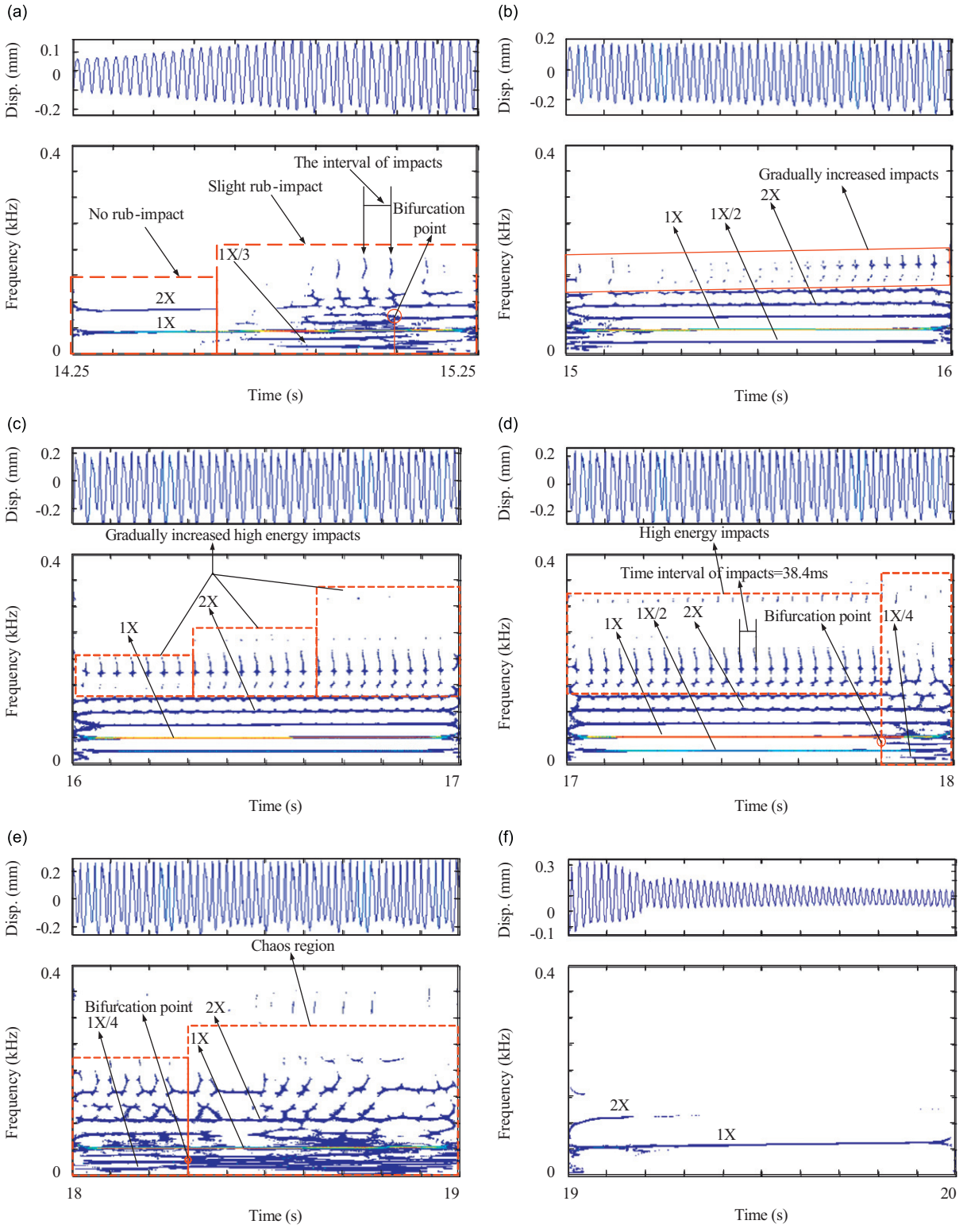

Fig. 10. Reassigned wavelet scalograms with crack and rub-impact fault in different rotational speed ranges.

Fig. 11 shows the rotor trajectories in four different rotational speed ranges. The rotor trajectory in Fig. 11(a) is a gradual increscent ellipse, which moves counter-clockwise and forward without rub-impact and backward when the rub-impact occurs and the points 1 and 2 in trajectory move outwards. In Fig. 11(b), the rotor trajectory is a two nested "8" shape curve. In Fig. 11(c), the two "8" shaped curves move towards center and a chaotic band of lines is induced when the rub-impact becomes serious. In the last figure, the rotor trajectory is converted to a regular ellipse and moves forward when the rotor system breaks away from its rub-impact.

The frequency amplitudes in two rotational speed ranges are illustrated in Fig. 12. The frequency spectrum is mainly composed of $\frac{1}{2}$-based fractional harmonic components and $1X/4$ can also be observed with small amplitude, as shown in Fig. 12(a). The spectrum lines are continuous except $1X/2$, $1X$, $3X/2$, $2X$, and $3X$, as

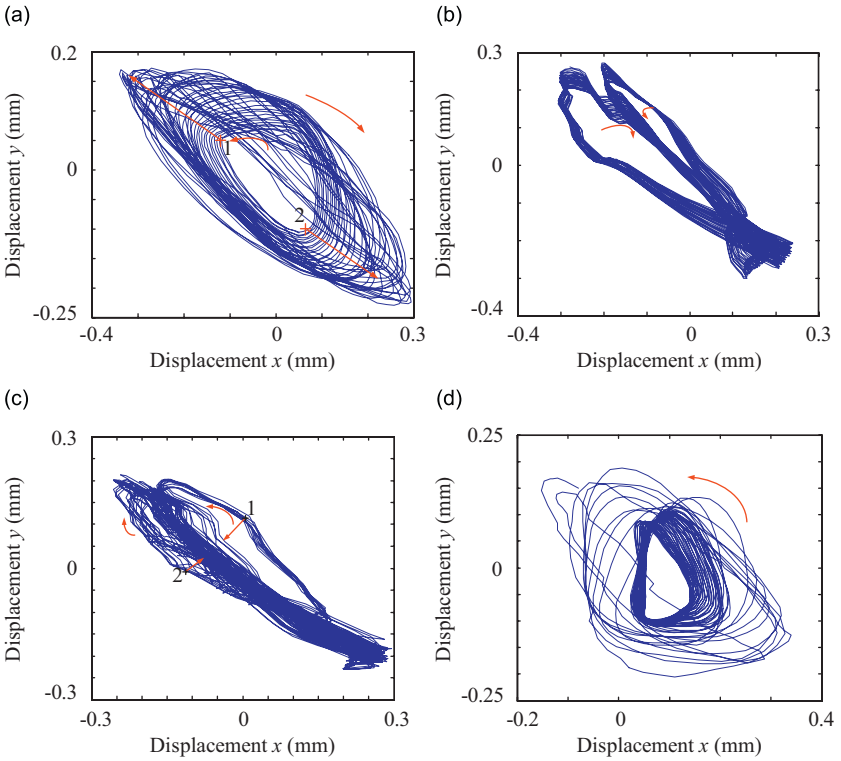

Fig. 11. Rotor trajectories of crack coupled with rub-impact faults in four different rotational speed ranges.

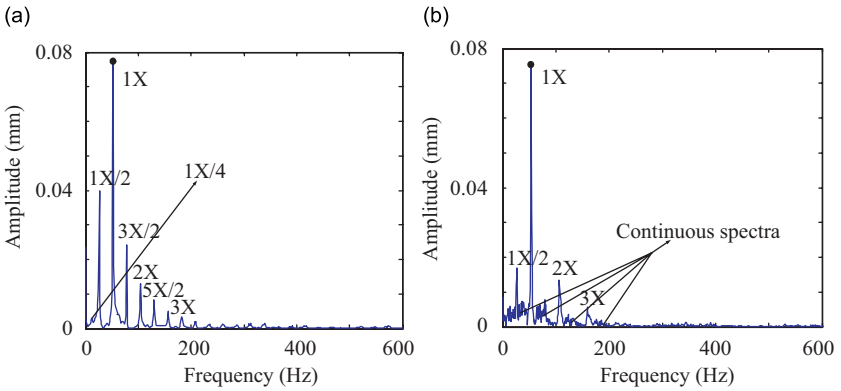

Fig. 12. Frequency amplitudes of crack coupled with rub-impact faults in two different rotational speed ranges.

Table 3
Feature comparison of crack, rub-impact and coupling of both.

Feature form	Fault extent	Fault types		
		Crack	Rub-impact	Crack coupled rub-impact
Time–frequency feature	Slight	$2X$	$2X$, $3X$, $4X$, $5X$, $6X$	$1X/3$, $2/3X$, $4X/3 \rightarrow 1X/2$, $3/2X$, $5/2X \rightarrow 1X/4$, $3/4X$
			Low energy impacts	High energy impacts
	Serious		IFC, CNC, $2X$, $3X$, $4X$, $5X$, $6X$	IFC, CNC, $2X$, $3X$ and irregular impacts
Rotor trajectory	Slight	Forward motion	Forward motion	Backward motion
	Serious		Backward motion	Backward motion

IFC—irreducible frequency component, CNC—colored noise component.

Table 4
An experimental description of oil-film instability coupled with bearing rub-impact.

Analysis method	Figures order number	Time range (s)	Rotational speed range (rev/min)
Spectrum cascade	Fig. 13	0–166.9	0–10488
Reassigned wavelet scalogram	Fig. 14(a)	49–50	7617–7735
	Fig. 14(b)	52–53	7969–8086
	Fig. 14(c)	58–59	8555–8613
	Fig. 14(d)	59–60	8613–8672
	Fig. 14(e)	73–74	9665–9723
	Fig. 14(f)	99–100	10 488–10 430
Rotor trajectory	Fig. 15(a)	49–50	7617–7735
	Fig. 15(b)	52–53	7969–8086
	Fig. 15(c)	58–59	8555–8613
	Fig. 15(d)	99–100	10 488–10 430
Amplitude spectrum	Fig. 16(a)	58–59	8555–8613
	Fig. 16(b)	73–74	9665–9723

10 488–10 430 denotes rotational speed changing from 10 488 to 10 430 rev/min.

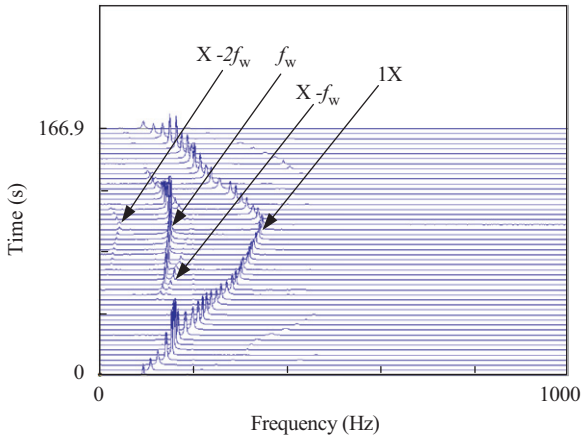

Fig. 13. Spectrum cascades of oil-film instability coupled with bearing rub-impact in both the speeding up and slowing down process.

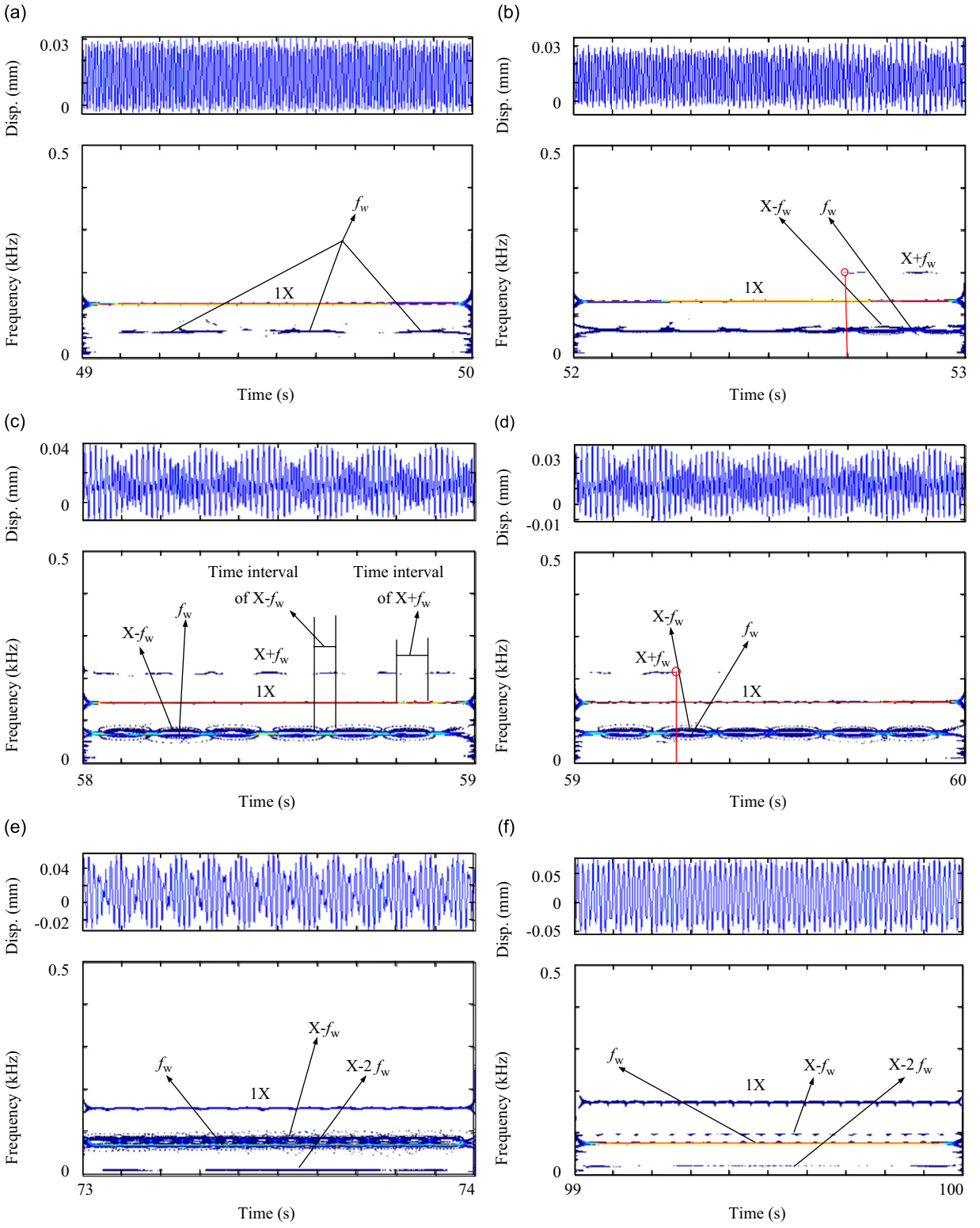

Fig. 14. Reassigned wavelet scalograms of oil-film instability coupled with bearing rub-impact in different rotational speed ranges.

shown in Fig. 12(b). The appearance of continuous spectra here can also be regarded as evidence of chaotic motion of the rotor system.

4.4. Comparison of fault feature of crack, rub-impact, and coupling of both

Based on the above analysis, the feature comparisons of the crack, rub-impact, and the coupling of both are tabulated in Table 3. Some novel fault features are summarized as follows: for the crack coupled with rub-impact fault, we discovered the route to and out of chaos, which starts from period-three (P3) motion, transits to period-two (P2) motion, period-four (P4) motion, chaotic motion, and finally to period-one (P1) motion, corresponding to the process of starting from slight rub-impact, transit to serious rub-impact, finally to no rub-impact. The slight rub-impact induces $\frac{1}{3}$-, $\frac{1}{2}$-, and $\frac{1}{4}$-based fractional harmonic components, and the serious rub-impact can introduce irreducible and colored noise frequency components to the spectrum. The above results present a good supplement to the studies of Chu [4] by showing a chaotic path with changing rotational speed.

As far as the system motion is concerned, the two types of faults can be distinguished by quasi-periodic motion for single rub-impact and chaotic motion for crack coupled rub-impact. Due to the coupling of two strong nonlinear factors, crack and rub-impact, we can conclude that the latter presents more complicated motion and phenomena in time–frequency domain.

5. Time–frequency features of oil-film instability coupled with bearing rub-impact

A comprehensive experimental description of all figures about oil-film instability coupled with bearing rub-impact is described in Table 4. Corresponding spectrum cascade is shown in Fig. 13, where rational frequency component $1X$, oil-film instability frequency component f_w, and combined frequency components of both can be observed. By using reassigned wavelet scalogram, the detailed fault features are depicted in Fig. 14.

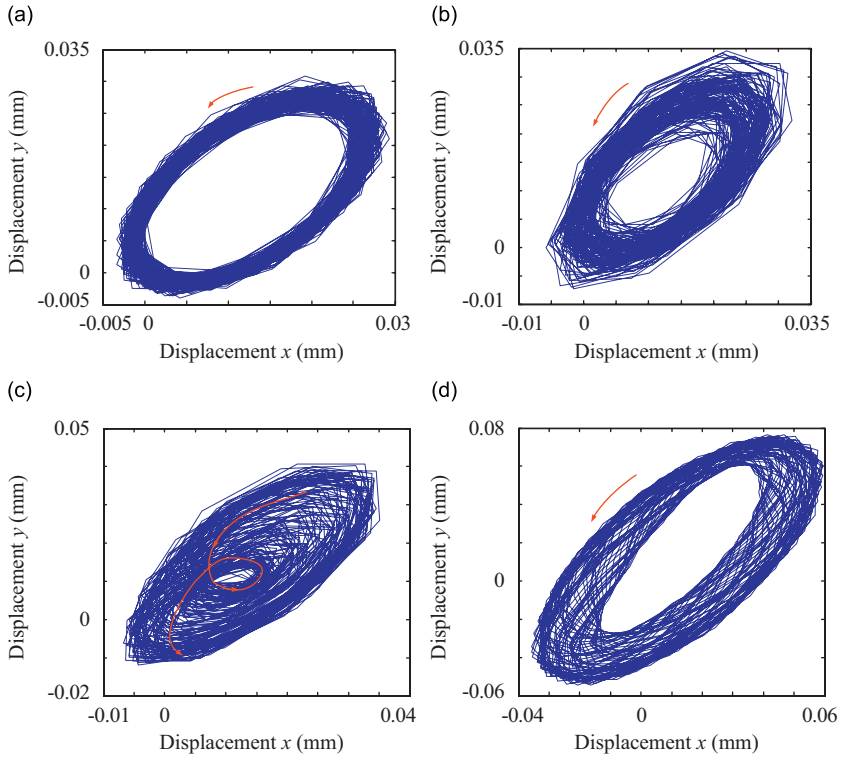

Fig. 15. Rotor trajectories of oil-film instability coupled bearing rub-impact under different rotational speed ranges.

Figs. 14(a)–(f) show the reassigned wavelet scalograms in some different rotational speed ranges. Oil whirl occurs and the intermittent oil whirl frequency component f_w can be observed near 49.1 s in Fig. 14(a). The whirl amplitude increases and slight bearing rub-impact phenomenon occurs with the increase of rotational speed, as shown in Fig. 14(b). The combined frequency component $X+f_w$ occurs near 52.7 s and $X-f_w$ close to f_w is also observed in the low frequency region. Beating vibration and alternate appearance of $X+f_w$ and $X-f_w$ can be observed in time-domain waveform and time–frequency plane, respectively, with the slow increase of the rotational speed, as shown in Fig. 14(c). These features show that the impacting and rubbing between rotor and bearing occur in turn. With continuous speeding up, the vibration amplitudes of frequency component $X+f_w$ decreases while $X-2f_w$ increases, and the space between frequency component f_w and $X-f_w$ also increases, as shown in Figs. 14(d) and (e). These features suggesting the impact has been weakened and the rubbing has been enhanced. When the rotational speed increases to the maximum value of 10 400 rev/min, as shown in Fig. 14(f), the oil whirl turns into the oil whip. The whip frequency is unchanged, but its vibration

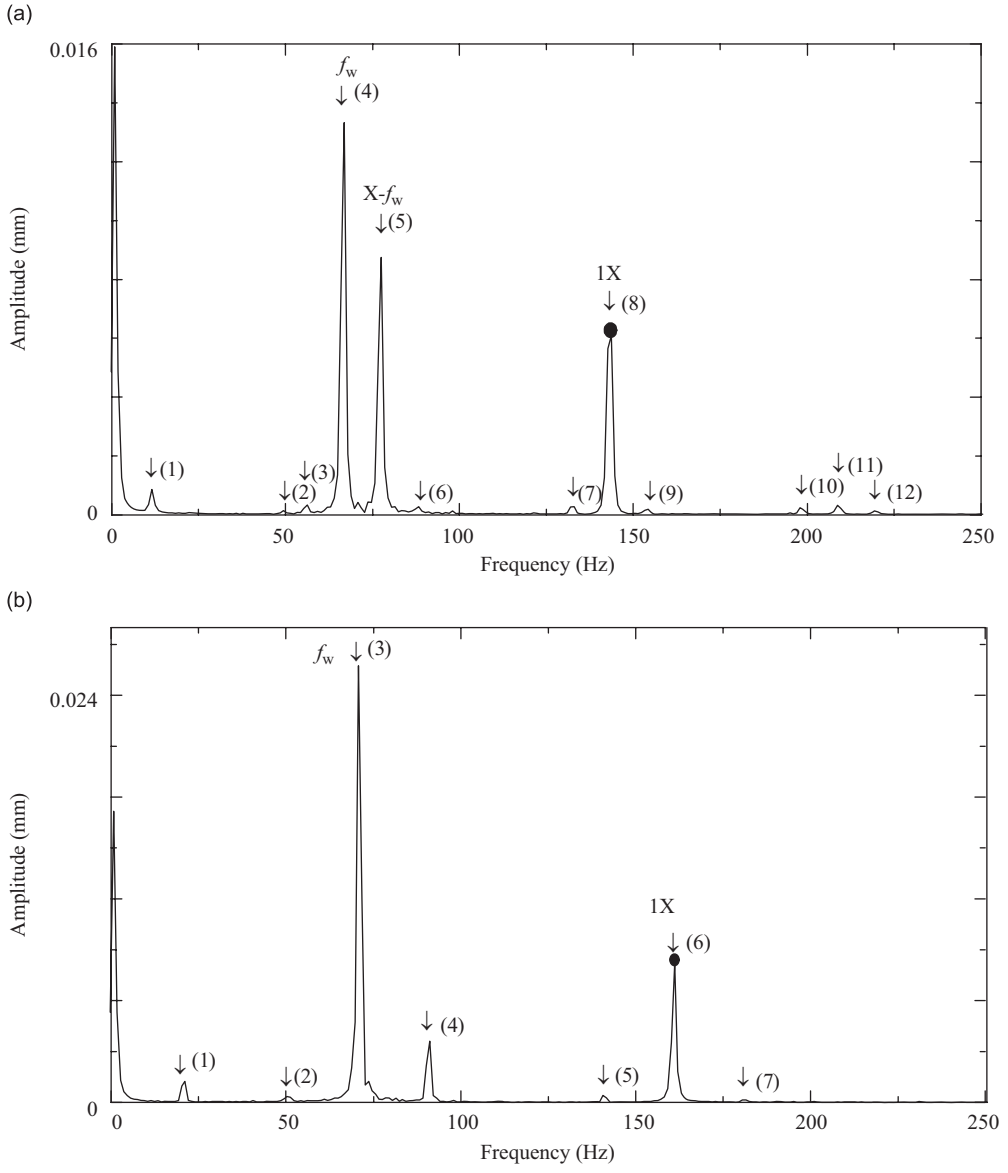

Fig. 16. Amplitude spectra of oil-film instability coupled with bearing rub-impact in two rotational speed ranges.

Table 5
Detailed combination frequency components in Fig. 16.

Figures order number	Frequency value (Hz)	Combination form	Amplitude value (μm)
Fig. 16(a)	(1) 10.7	$X-2f_w$	0.912
	(2) 47.9	$X/3$	0.129
	(3) 55.7	$3f_w-X$	0.352
	(4) 66.4	f_w	14.531
	(5) 77.1	$X-f_w$	9.537
	(6) 87.9	$2X-3f_w$	0.278
	(7) 132.8	$2f_w$	0.280
	(8) 143.6	X	6.628
	(9) 154.3	$2X-2f_w$	0.181
	(10) 199.2	$3f_w$	0.230
	(11) 210.0	$X+f_w$	0.319
	(12) 220.7	$2X-f_w$	0.123
Fig. 16(b)	(1) 20.5	$X-2f_w$	1.231
	(2) 49.8	$3f_w-X$	0.360
	(3) 70.3	f_w	25.843
	(4) 90.8	$X-f_w$	3.614
	(5) 140.6	$2f_w$	0.406
	(6) 161.1	X	8.242
	(7) 181.6	$2X-2f_w$	0.134

amplitude increases. Also, frequency component $X-f_w$ is far from f_w so that the beating vibration disappears in the time-domain waveform.

The rotor trajectories in four different rotational speed ranges are shown in Fig. 15. Fig. 15(a) shows the rotor trajectory when only oil whirl appears. The motion of the rotor system is counter-clockwise forward and limited in a ring belt. The ring belt of rotor motion appears to be wider, with motion direction remaining unchanged in the stage of slight bearing rub-impact, as shown in Fig. 15(b). With the increase of rotational speed, the bearing rub-impact increasingly worsens and the rotor trajectory is an inner "8" shape; its motion direction is shown in Fig. 15(c). The rotor motion is extended to an elliptic surface. The irregular rotor motion suggests rub-impact aggravating. When oil whip occurs, vibration amplitude increases and multiple nested ellipses can be observed when rotational speed is up to 10 400 rev/min. At this time, the serious rub-impact occurs and the rotor motion is away from center, as shown in Fig. 15(d).

To obtain the detailed frequency information, the data in 58–59 s and 73–74 s is analyzed by using frequency spectrum and the results are shown in Fig. 16 and Table 5. The amplitude modulation phenomenon is obvious by analyzing the frequency components. Four group frequency components (f_w, X, $2X-f_w$), ($X-f_w$, X, $X+f_w$), ($2X-3f_w$, X,$3f_w$), and ($2f_w$, X, $2X-2f_w$) can cause amplitude modulation, where the carrier frequency is X and the modulation frequencies are $X-f_w$, f_w, $3f_w-X$, and $X-2f_w$, respectively. The frequency spectrum is given in Fig. 16(b) when the rub-impact becomes serious. The combination frequency components decrease in comparison to Fig. 16(a). One group of frequency components, ($2f_w$, X, $2X-2f_w$), can cause amplitude modulation. $X-2f_w$ vibration amplitude increases with gradual aggravation of the rub-impact.

In the above analysis of oil-film instability coupled with bearing rub-impact, some interesting fault features are summarized as follows: In the stage of slight rub-impact, the plentiful combined frequency components of X (rotating frequency) and f_w (oil-film instability frequency) can be observed. The regular alternate appearance of $X+f_w$ and $X-f_w$ indicates the change between impacting and rubbing. Moreover, amplitude modulation phenomenon is also observed. The carrier frequency is X and the modulation frequencies are $X-f_w$, f_w, $3f_w-X$, and $X-2f_w$, respectively. In the stage of serious rub-impact, the vibration amplitude of f_w increases, the high combined frequency components disappear, and the vibration amplitude of low frequency component $X-2f_w$ increases. These features can be viewed as the most distinguishable character of oil-film instability coupled with serious bearing rub-impact.

6. Conclusions

In this study, the crack coupled with rub-impact fault and the oil-film instability coupled with bearing rub-impact fault are simulated by using a rotor test rig. By combining spectrum cascade, reassigned wavelet scalogram, rotor trajectory, and frequency spectrum, some novel and interesting phenomena are discovered. For the crack coupled with rub-impact fault, the system motion is from period-three motion to period-two motion and period-four motion to chaotic motion when the rub-impact is from slight rub-impact to serious rub-impact. For the oil-film instability coupled with bearing rub-impact, various combinations of the rotating frequency and the oil-film instability frequency can be observed. The combined frequency components decrease and vibration amplitude of the lowest rotational frequency component increases with increasingly worsening bearing rub-impact. Regardless of the slight bearing rub-impact or the serious bearing rub-impact, the vibration amplitudes of the combined frequencies are less than those of the rotating frequency and the oil-film frequency, which shows that the oil-film instability plays a dominant role in the coupled fault.

Acknowledgments

We are grateful to the National 863 Project (Approval no. 2007AA04Z442) and the China Natural Science Funds (NSFC, Grant nos. 50805019, 50775028, 50775025 and 50805046) for providing financial support for this work.

We would like to express our gratitude to all those who made completion of this paper possible. We want to thank all the teachers of the Institute of Mechanical Design and Theory for providing help in carrying out experimental research from the beginning. We have furthermore to thank Professor John Paddison, Professor Huang Xianli, Professor Li Dongxu, and Professor Zheng Ling for revising the final version of the paper for English style and grammar, and for offering suggestions for improvement.

We are deeply indebted to our supervisor Professor Wen Bangchun whose help, stimulating suggestions, and encouragement helped us in all the time in the research and writing of this paper. Especially, we would like to give our special thanks to all the anonymous reviewers whose comments and advice enabled us to greatly improve the quality of the paper.

References

[1] A. Muszynska, P. Goldman, Chaotic responses of unbalanced rotor/bearing/stator systems with looseness or rubs, *Chaos, Solutions & Fractals* 5 (9) (1995) 1683–1704.

[2] W.M. Zhang, G. Meng, D. Chen, J.B. Zhou, J.Y. Chen, Nonlinear dynamics of a rub-impact micro-rotor system with scale-dependent friction model, *Journal of Sound and Vibration* 309 (2008) 756–777.

[3] H.C. Piccoli, H.I. Weber, Experimental observation of chaotic motion in a rotor with rubbing, *Nonlinear Dynamics* 16 (1998) 55–70.

[4] F.L. Chu, W.X. Lu, Experimental observation of nonlinear vibrations in a rub-impact rotor system, *Journal of Sound and Vibration* 283 (2005) 621–643.

[5] X. Dai, Z. Jin, X. Zhang, Dynamic behavior of the full rotor/stop rubbing: numerical simulation and experimental verification, *Journal of Sound and Vibration* 251 (5) (2002) 807–822.

[6] N. Bachschmid, P. Pennacchi, A. Vania, Identification of multiple faults in rotor systems, *Journal of Sound and Vibration* 254 (2) (2002) 327–366.

[7] Y.G. Luo, Z.H. Ren, H. Ma, T. Yu, B.C. Wen, Stability of periodic motion on the rotor-bearing system with coupling faults of crack and rub-impact, *Journal of Mechanical Science and Technology* 21 (6) (2007) 860–864.

[8] B.C. Wen, X.H. Wu, Q. Ding, et al., *Theory and Experiment of Nonlinear Dynamics for Rotating Machinery with Faults*, Science Press, Being, 2004, pp. 112–124 (in Chinese).

[9] F.Y. Wan, Q. Y Xu, S.T. Li, Vibration analysis of cracked rotor sliding bearing system with rotor-stator rubbing by harmonic wavelet transform, *Journal of Sound and Vibration* 271 (2004) 507–518.

[10] F.Q. Wu, G. Meng, Compound rub malfunctions feature extraction based on full-spectrum cascade analysis and SVM, *Mechanical Systems and Signal Processing* 20 (2006) 2007–2021.

[11] Z.K. Peng, F.L. Chu, Application of the wavelet transform in machine condition monitoring and fault diagnostics: a review with bibliography, *Mechanical Systems and Signal Processing* 18 (2004) 199–221.

[12] F. Auger, P. Flandrin, Improving the readability of time–frequency and time-scale representations by the reassignment method, *IEEE Transactions on Signal Processing* 43 (5) (1995) 1068–1089.

[13] F. Auger, P. Flandrin, P. Gongcalves, O. Lemonice, *Time–frequency Toolbox Tutorial*, CNRS, France, Rice University, USA, 1997.

[14] Q.K. Han, H.L. Yao, Z.W. Zhang, et al. Experiment of oil-film whirl in rotor system and wavelet fractal analyses, *ASME 2005 International Design Engineering Technical Conferences*, CA, USA, 2005.
[15] S.A. Adewusi, B.O. Al-bedoor, Wavelet analysis vibration signals of an overhang rotor with a propagating transverse crack, *Journal of Sound and Vibration* 246 (5) (2001) 777–793.
[16] A.K. Darpe, A novel way to detect transverse surface crack in a rotating shaft, *Journal of Sound and Vibration* 305 (2007) 151–171.
[17] B. Yang, C.S. Suh, A.K. Chan, Characterization and detection of crack-induced rotary instability, *Journal of Vibration and Acoustics* 124 (2002) 40–48.
[18] P.W. Tse, Y.H. Peng, R. Yam, Wavelet analysis and envelope detection for rolling element bearing fault diagnosis, *Journal of Vibration and Acoustics* 123 (2001) 303–310.
[19] Z.K. Peng, F.L. Chu, Y. He, Vibration signal analysis and feature extraction based on reassigned wavelet scalogram, *Journal of Sound and Vibration* 253 (2002) 1087–1100.
[20] Z.K. Peng, F.L. Chu, P.W. Tse, Detection of the rubbing-caused impacts for rotor-stator fault diagnosis using reassigned scalogram, *Mechanical Systems and Signal Processing* 19 (2005) 391–409.
[21] I.W. Mayes, W.G.R. Davies, The vibrational behavior of a rotating shaft system containing a transverse crack, *I Mech E Conference Publication*, *Vibration in Rotating Machinery*, *Paper No. C168/76*, 1976.
[22] R. Gasch, Dynamic behavior of a simple rotor with a cross-sectional crack, *I Mech E Conference Publication*, *Vibration in Rotating Machinery*, *Paper No. C178/76*, 1976.
[23] I.W. Mayes, W.G.R. Davies, A method of calculating the vibrational behavior of coupled rotating shaft containing a transverse crack, *I Mech E Conference Publication*, *Vibration in Rotating Machinery*, *Paper No. C254/80*, 1980.